Jordan Journal of Civil Engineering, Volume **16**, No. **4**, **2022**

Automated Seismic Design of Planar Frames Blending Structural Reliability and Heuristic Optimization

Laura Niño Sepúlveda [1)*], ***Laureen Carvajal Oyaga*** [1)], ***David Cotes Prieto*** [1)], ***Camilo Cotes Prieto*** [2)] ***and Oscar Begambre*** [1)]

[1)] School of Civil Engineering, Universidad Industrial de Santander, Bucaramanga, Colombia.
* Corresponding Author. E-Mails: laura.nino@correo.uis.edu.co; laureen.carvajal1@correo.uis.edu.co; dscotpri@correo.uis.edu.co; ojbegam@uis.edu.co
[2)] School of Civil, Environmental and Land Management Engineering, Politecnico di Milano, Milan, Italy.
E-Mail: ivancamilo.cotes@mail.polimi.it

ABSTRACT

This study presents a robust reinforced concrete planar frame automated seismic design procedure incorporating reliability analysis and heuristic optimization. The limit-state function selected corresponds to the story drift. In order to reduce the computational burden and make a real-life practical application, the response surface method was employed to obtain the limit-state function. Then, two methods, the Hasofer-Lind and Rackwitz-Fiessler and the Monte Carlo simulation, were applied to determine the reliability index β. The story drift limit-state was evaluated using linear elastic analysis in a reinforced concrete planar frame with five stories and three spans under gravitational and seismic loads, including all sway special moment frame constraints, as per the Colombian code for seismic-resistant buildings NSR-10. The weight of the reinforced concrete planar frame was minimized by employing particle-swarm optimization and a genetic algorithm, considering its cross-sections and longitudinal reinforcement as discrete optimization variables. Two general optimization scenarios developed in the software MATLAB® 2019b were considered: (I) including a minimum β as a design constraint and (II) without including a minimum β as a design constraint. For scenario (I), the compressive strength of concrete and the seismic load were considered random variables. The results show an increase in the weight of the reinforced concrete planar frame for scenario (I) of 11.63% (Hasofer-Lind and Rackwitz-Fiessler) and 16.89% (Monte Carlo simulation) when compared to scenario (II).

Nonetheless, β values for scenario (I) were 1.534 (Hasofer-Lind and Rackwitz-Fiessler) and 1.713 (Monte Carlo simulation), which were significantly higher than the 0.065 β-value for scenario (II). In conclusion, in all design examples, achieving satisfactory reliability levels (β) means increasing the cross-sectional area of the reinforced concrete planar frame beyond the Colombian code for seismic-resistant buildings, NSR-10, minimal requirements. Finally, from the structural safety point of view, the presented procedures permit fast reinforced concrete planar frame designs incorporating reliability analysis and heuristic optimization with good computational times.

KEYWORDS: Reinforced concrete structures, Heuristic optimization, Particle-swarm optimization, Genetic algorithm, Reliability index, Response surface method, HL-RF method, Monte Carlo simulation.

INTRODUCTION

Reinforced concrete is one of the most used materials in the construction industry (Aguirre-Guerrero and Mejía de Gutiérrez, 2020); the demand for this material has increased over the years. Its current global annual production is estimated at around 25 billion tons (Martinez Molina et al., 2015). High production of this material negatively impacts the environment; so optimization plays a vital role in minimizing material

Received on 8/10/2021.
Accepted for Publication on 21/7/2022.

consumption, therefore maximizing the environmental sustainability of infrastructure works. Optimization aims to minimize or maximize an objective function to get a feasible solution.

Historically, classic optimization methods, such as Newton's, maximum slope or Levenberg-Marquart methods (Negrin et al., 2019), have been used. Nonetheless, these methods require differentiability of the objective functions and tend to get stuck in local optimum values, limiting their use to simple academic structural problems. Actual structural optimization problems are usually described by non-differentiable objective functions and have multiple optimal solutions, making them more complex. As a result, the implementation of heuristic optimization, HO, methods such as particle-swarm optimization, PSO, genetic algorithm, GA, simulated annealing and ant-colony optimization, among others, has highly increased structural design optimization (Li and Liu, 2009). These methods are based on the generation of multiple random scenarios for the optimization variables, called candidate solutions, and through mathematical programming techniques, achieve the optimization process, even providing better solutions in contrast to classic optimization methods (Kunche and Reddy, 2016; Li and Liu, 2011).

Moreover, structural design optimization is a constrained problem, since the solution must satisfy the design code and constructability requirements; therefore, hybrid methods and penalty functions (and penalty parameters) must be used to incorporate constraints in the objective function (Ab. Aziz et al., 2011). Many authors have implemented constrained HO in structural design. Rajeev and Krishnamoorthy (1992) successfully implemented the GA algorithm in the weight minimization of truss structures, highlighting the advantage of HO in handling discrete optimization variables. The computational cost of implementing this algorithm was higher than those of classical methods; however, this is not a limitation due to current computational capacities. Dillen et al. (2021) implemented GA to minimize the weight of an actual market-hall steel structure incorporating the requirements of the local structural design code as constraints. They assessed a reduction of 15% in the required material for the structure compared to the actual non-optimized conventional design. The researchers socialized the optimization results with the original structural designers allowing them to conclude that exists an interest in the industry in implementing structural optimization; nonetheless, the lack of practical tools, automatically blending it into structural analysis and design, discourages its massive use.

Research studies have evidenced many advantages due to implementing structural optimization; nevertheless, most of these consider the variables and parameters as deterministic, dismissing their stochastic nature. That becomes a problem, since it has been found that deterministic optimization could yield structures with high probabilities of failure due to the statistical uncertainties related to the optimization variables. For instance, Danesh (2019) evaluated the probability of failure of moment-resisting steel frames with special ductility designed using four different HO methods to minimize the material cost. The stochastic variables considered were the yield strength and modulus of elasticity of the steel and the seismic pseudo-acceleration demand. He found that although the weight was minimized, the probability of serious damage in the frames due to severe earthquakes highly increased, which may lead to lifecycle overcosts in the structures. Therefore, it was recommended to perform the optimization incorporating stochastic components to reduce failure probabilities.

Hence, a more realistic approach to the optimal design process incorporates the statistical uncertainty associated with the different variables involved, by which it is possible to estimate the probability of a structure exceeding a particular limit state. This procedure is known as reliability analysis, RA (Grubišić et al., 2019) and aims to determine the probability of failure, p_f, defined as the probability that the demand will exceed the capacity, which alternatively can be more conveniently represented by the reliability index, β. The limit-state function expresses the relationship between capacity and demand, which can be explicit or implicit concerning variables considered random.

For actual structures, such as buildings, the limit-state function is complex and implicit, which involves high computational costs in the calculation of β. However, it is possible to approximate an explicit function through procedures, such as the response surface method RSM (Tan et al., 2013). β can be estimated using different methods, such as Monte Carlo

simulation, MCS, Latin Hypercube or the Hasofer-Lind and Rackwitz-Fiessler method, HL-RF. The method selection usually depends on the complexity of the analyzed-limit state function.

Current design codes generally employ safety factors to prevent demand from exceeding the structure's capacity, increasing loads and decreasing resistance, leading to very conservative designs. In this context, as stated by Rastegaran et al. (2022), it is necessary to develop algorithms that facilitate, for designers and project owners, the incorporation of RA in the optimal structural design as a decision-making tool. Today, practical structural optimization usually does not incorporate structural RA, leading to a lower reliability index than recommended values (Danesh, 2019; Faes and Valdebenito, 2020). Hence, researchers, such as Peng et al. (2021), have pointed out the importance of considering the RA in the structural-design optimization process that allows the compensation between risk and benefit.

The literature review shows that optimization is a powerful tool for structural design; nonetheless, there are issues to improve in order to promote its safe and massive use. Therefore, this research aims to encourage the use of optimization in the industry through the following contributions: (i) the development of a robust, practical tool with automated seismic-design procedures (ASDP), including structural seismic analysis and optimized design of cross-section dimensions, as well as longitudinal and transverse steel reinforcement (rebar diameter and amount), following the requirements of the Colombian code for seismic-resistant buildings-NSR-10 (Ministerio de Ambiente Vivienda y Desarrollo Territorial, 2017); (ii) the incorporation of reliability analysis as a constraint in the process of optimal design of planar reinforced concrete frames and (iii) the comparison between a purely deterministic (without reliability analysis) optimal automatic structural design and an optimum RA structural design (that ensures the desired safety).

The ASDP automatically carries out the structural analysis and determines the sizes of cross-sections and longitudinal and transverse reinforcements through heuristic-optimization techniques avoiding local optima. Two approaches to the ASDP optimization were considered. One ASDP includes deterministic HO (without reliability analysis), here referred to as ASDO (Automatic Seismic Design Optimization) and the other is blending ASDP with RA and HO methods, referred to as ASDO-RA (Automatic Seismic Design Optimization with Reliability Analysis). The objective function employed was the weight of reinforced concrete planar frame (RCPF) and the optimization variables (OV) corresponded to the cross-section dimensions and the cross-sections' longitudinal reinforcement (rebar). The HO methods implemented in this work were GA and PSO. Regarding RA, sources of uncertainty for the story drift limit state, SDLS, were the seismic force (F_s) and the reinforced concrete strength (f_c'). In order to evaluate a computationally less expensive alternative than MCS, β was also calculated using the HL-RF method. In the ASDO-RA, a minimum value of β, calculated using the HL-RF and the MCS methodologies, is incorporated as a design constraint (see Table 4). The ASDO and ASDO-RA minimize the weight of a real RCPF located in a high seismic-demand zone designed following the Colombian code for seismic-resistant buildings NSR-10 (Ministerio de Ambiente Vivienda y Desarrollo Territorial, 2017). The impact of using ASDO-RA was assessed by contrasting its minimum weight results and reliability indices with those obtained from a conventional design (engineering office work) and ASDO.

The outline of this work is as follows: the ASDO and ASDO-RA used in this work are defined in the next section. It includes the RCPF description, the employed seismic analysis techniques and the optimization-problem formulation based on structural RA and HO methods. Then, a numerical assessment of ASDO-RA is described and compared against ASDO and the conventional structural design of the RCPF. The final observations, conclusions and limitations are presented thereafter. Finally, in the last section, recommendations for future studies are presented.

AUTOMATED SEISMIC DESIGN PROCEDURES - ASDP

RCPF DESCRIPTION

In this study, the structure analyzed (designed and optimized) consisted of an RCPF as part of an actual building. The building has five stories and three spans constituted by 15 beams and 20 columns, as seen in Fig.1 and it is located in the metropolitan area of Bucaramanga, Colombia.

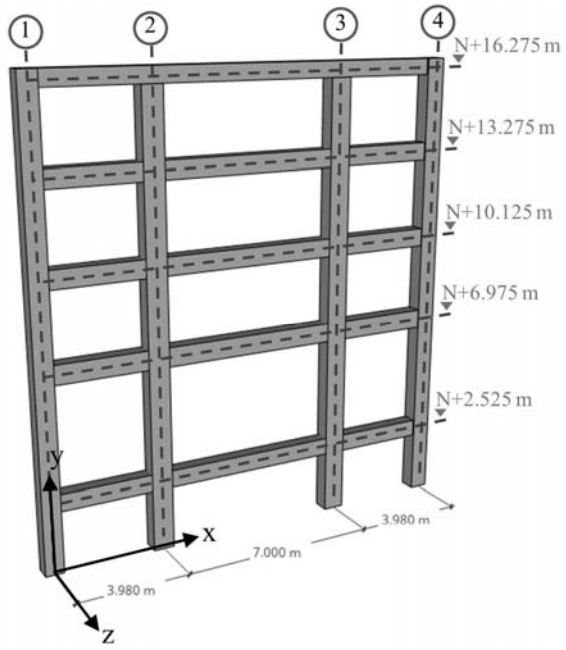

Figure (1): Planar frame

The analysis and structural design were developed following the requirements of the Colombian code NSR-10 (Ministerio de Ambiente Vivienda y Desarrollo Territorial, 2017). The structure is in a high seismic-demand zone; so it requires a special energy-dissipation capacity, SED, and was assumed to be founded on type C ground, corresponding to very dense ground or soft rock. Concrete compressive strength, f_c', was 21 MPa and the elasticity modulus, E_c, was according to section C.8.5.1 of the NSR-10 for normal-density concrete corresponding to Equation 1 (Ministerio de Ambiente Vivienda y Desarrollo Territorial, 2017),

$$E_c = 4700\sqrt{f_c'} \quad (1)$$

Steel yield strength, f_y, was 420 MPa corresponding to the elasticity modulus, E_s, equal to 200 GPa. Structural analysis and design were developed based on the optimization variables set out in each candidate solution (x).

RCPF Structural Analysis and Design

Load Analysis

The RCPF was subjected to the actions of dead loads, D, live loads, L and seismic force, F_s, all in the XY plane (see Fig. 1).

Gravitational Loads

The load estimation was based on the distribution of slab system of a story type of the whole building, considering the tributary width for gravitational load transfer to the RCPF, corresponding to axis D, (Fig. 2), obtaining a value of load transferred for the outer beams, between axes 1-2 and 3-4, and another value for the mid beams, between axes 2-3.

Table 1 presents the transferred dead loads' estimate, which included loads by (i) non-structural walls, (ii) floor topping, (iii) hydraulic, sanitary and electric networks and (iv) self-weight of joists and slabs. The weight of the structural elements (beams and columns) varied in each design, depending on the candidate solution by the HO method (dimensions of the cross-sections). The transferred live load was defined according to the area used as (v) balconies or (vi) private rooms and corridors.

Table 1. Gravitational loads transferred to the RCPF

	Mid-beams (Axes 2-3)	**Outer beams (Axes 1-2;3-4)**
Dead load [kN/m]		
(i)	16.245	16.245
(ii)	8.664	8.664
(iii)	1.083	1.083
(iv)	24.228	29.059
	50.220	55.051
Live load [kN/m]		
(v)	6.975	6.975
(vi)	7.236	7.236
	14.211	14.211

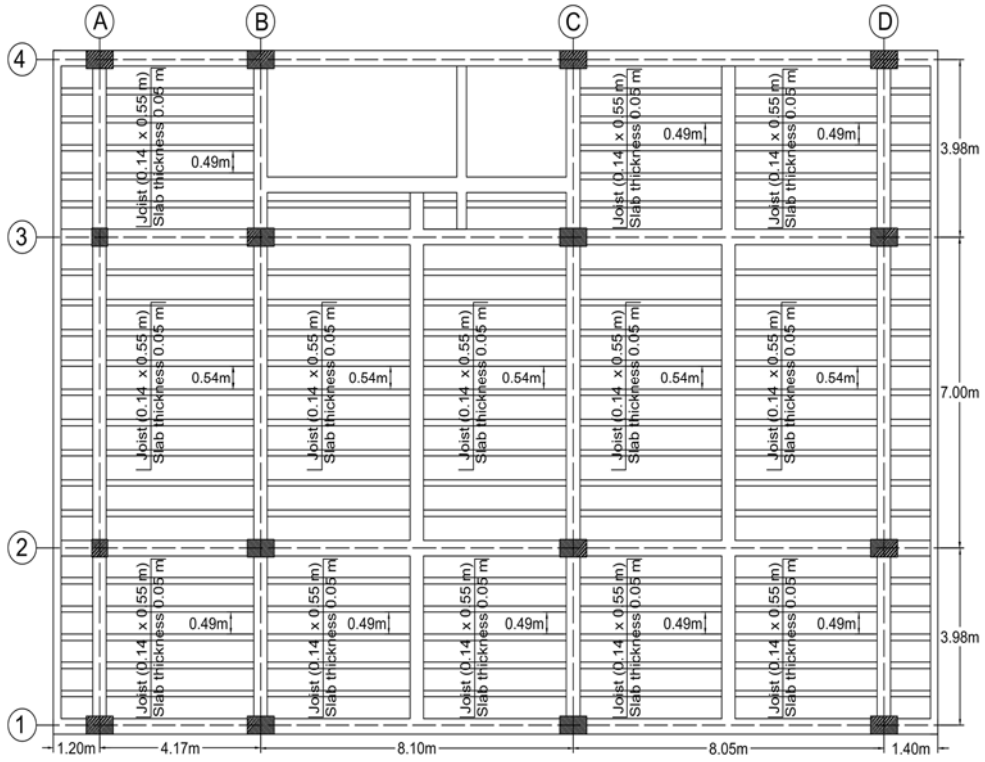

Figure (2): Floor-slab system of the real building

Table 2. Random variables

Random variable	PDF	Characteristic values
f_c'	Normal	$\mu = 21MPa$ $c.o.v = 0.10$
F_s	Log-normal	μ *depends on each candidate solution* $c.o.v = 0.31$

Seismic Force

Seismic force, F_s, estimation was made using the equivalent horizontal-force method, EHF, according to the NSR-10 (Ministerio de Ambiente Vivienda y Desarrollo Territorial, 2017, section A.3.4.2.1). The approximate fundamental period, T_a, determined by equation A.4.2-3 of the NSR-10 was equal to $0.5787\ s$. Equations A.4.3-2 and A.4.3-3 of the NSR-10 were used to determine the equivalent horizontal force on each story according to the shear base force, V_s and the acting dead loads on the RCPF, as shown in Fig. 3. The V_s was calculated based on spectral response acceleration, S_a, which was obtained from the design response spectrum presented in Fig. 4, where A_a, A_v, F_a and F_v correspond to effective peak horizontal acceleration coefficient, effective peak horizontal speed coefficient, short-period site coefficient and long-period site coefficient, respectively.

The ratio between F_s and the response modification coefficient, R, represents the design reduced seismic force, E. The coefficient R corresponds to the product of the basic energy dissipation coefficient, R_0 and the coefficients of reduction of energy-dissipation capacity by irregularities in height, ϕ_a and by the absence of redundancy, ϕ_r. R_0 was established as seven according to Table A.3-3 of the NSR-10, ϕ_p was set to 1, because the story type (Fig. 2) does not present any of the floor plant irregularities described in Table A.3-6 of the NSR-10; ϕ_r was set to 1, because it meets the redundancy conditions described in A.3.3.8.2 of the NSR-10 and ϕ_a is varied according to the candidate solution and the cases described in Table A.3-7 of the NSR-10 (Ministerio de Ambiente Vivienda y Desarrollo Territorial, 2017).

Drift

The maximum drift limit on reinforced concrete structures is set to 1% of the interstory height according to Table A.6.4-1 of the NSR-10 for linear analysis with non-cracked cross-sections. In order to determine the

maximum drift, $\Delta_{máx}$, the displacements of all the nodes of the RCPF under the action of F_s and D were calculated; the maximum drift was also expressed as a percentage of the story height. This procedure was performed using the direct stiffness method by implementing the programming code described later.

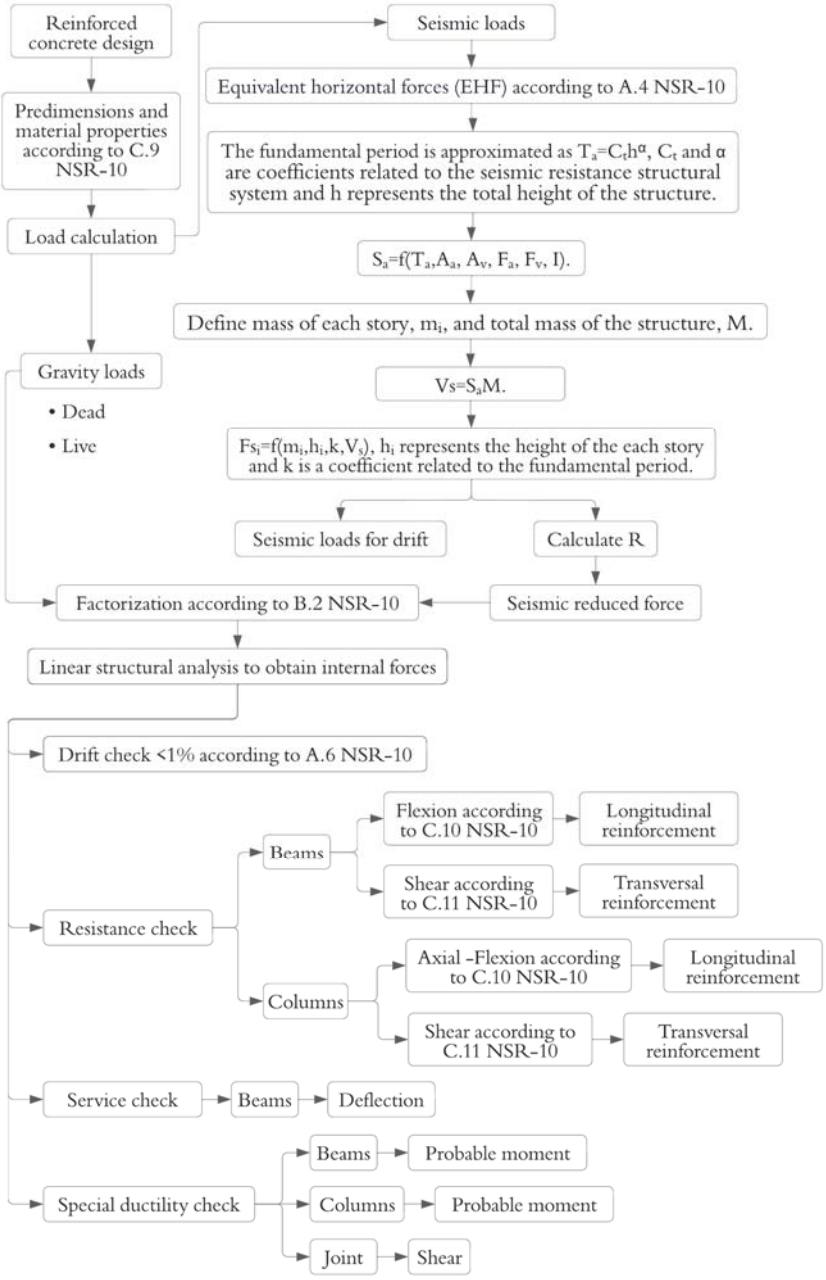

Figure (3): Flowchart of the reinforced-concrete design process

Load Combinations

The design of the structural elements was carried out under the combinations of factored loads, set out in section B.2.4.2 of the NSR-10, according to the following load combinations (D=dead: L=live; E= earthquake). Equations (2)-(7) for factored loads were taken from Ministerio de Ambiente Vivienda y Desarrollo Territorial (2017):

$$1.4D \quad (2)$$

$$1.2D + 1.6L \quad (3)$$

$$1.2D + L \quad (4)$$

$$1.2D + E + L \quad (5)$$

$$0.9D \quad (6)$$

$$0.9D + E \quad (7)$$

Structural Analysis

The internal forces and displacements of the structural elements, produced by the loads mentioned above, using the Timoshenko beam model (Luongo et al., 2021) and including the axial stiffness of the structural elements, were determined by the direct stiffness method. The structural analysis developed by the authors in the MATLAB® 2019b software was validated through the trial version of the SAP2000® v22 Software.

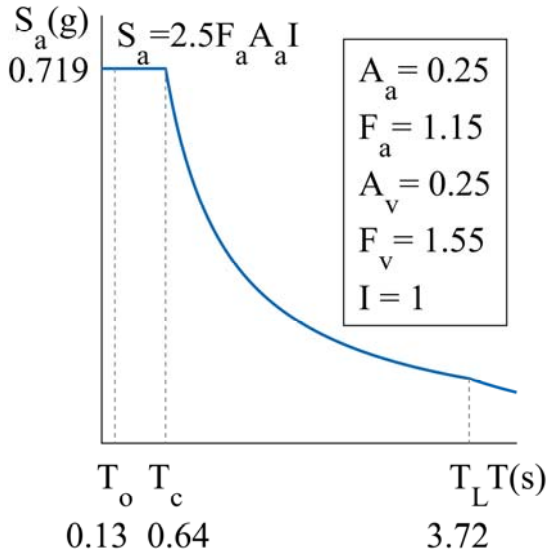

Figure (4): Design response spectrum

Design Loads

Each element's axial force, shear force and bending moment functions were calculated according to the internal forces obtained from the structural analysis for each load combination. The beam design forces (shear force and bending moment) in the three cross-sections of interest (initial, midspan and end sections) were determined using the load combination envelope. Column design forces corresponded to the axial force, shear force and bending moment obtained from structural analysis for each load combination, without considering the envelope due to the interaction between axial force and bending moment. The magnification process described in section C.10.10 of the NSR-10 was implemented for the bending moment in columns when it was impossible to ignore slenderness effects.

Structural Design

The structural elements were designed using the load and resistance factor design methodology, LRFD, which implies that the design strength of the sections was at least equal to the demand (Ministerio de Ambiente Vivienda y Desarrollo Territorial, 2017). The longitudinal rebar design in beams was performed by an iterative process of selecting the number of bars from a diameter commercially available (see candidate solutions). Also, a maximum of three longitudinal rebar lines was considered to meet the design criteria. The number of bars was set in the ranges [2-8] and [2-14] for positive and negative bending moment requests, respectively. In turn, longitudinal rebar in columns generated in the candidate solution was arranged seeking separations less than 150 mm to avoid additional demand of lateral support hookes. The transverse rebar design in beams and columns was performed following shear methodology by probable moments described in C.21.5.4 and C.21.6.5, respectively (Ministerio de Ambiente Vivienda y Desarrollo Territorial, 2017), using closed stirrups, 9.525 mm in diameter. Two spacings for the stirrups were calculated, one for the confined area (adjacent to the joints or where yielding due to bending may occur) and the second for the unconfined area. A flowchart with the design procedure and seismic force calculation is illustrated in Fig. 4.

Table 3. Optimization variables

OV	N°. OV	Description
1	5	Beams dimensions "y-axis", width, associated by story [mm].
2	5	Beams dimensions ratios "y/z-axes", ratio width/depth, associated by story.
3	30	Beams' positive and negative rebars [3.175 mm].
4	2	Columns dimensions "y-axis", width, associated by outer and mid axis (1-4 and 2-3) [mm].
5	2	Columns dimensions "x-axis", depth, associated by outer and mid axis (1-4 and 2-3) [mm].
6	2	The diameter of rebars in columns is associated with the outer and mid axis (1-4 and 2-3) [3.175 mm].
7	20	Amounts of rebar in columns.

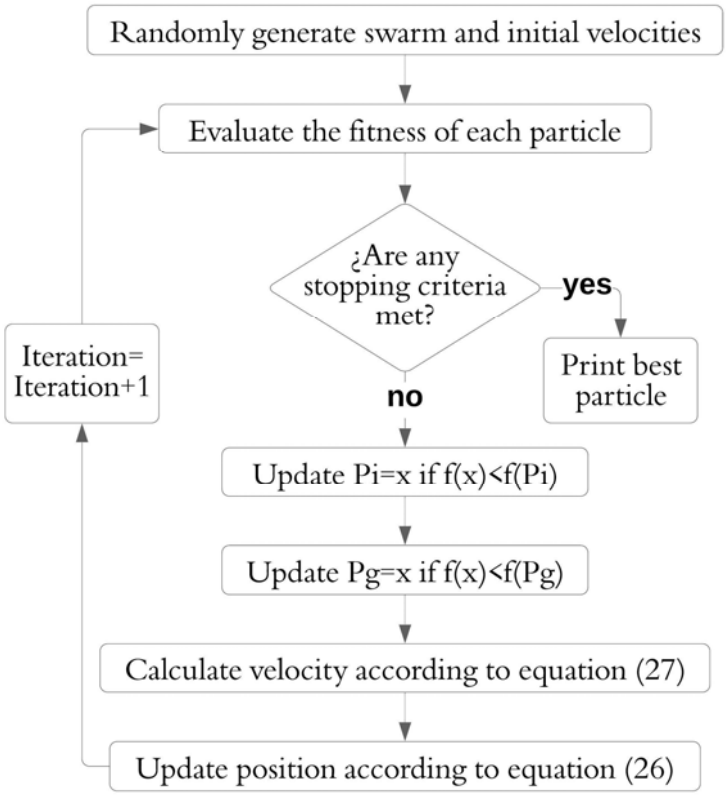

Figure (5): PSO flowchart

Structural Reliability

The structural reliability of the RCPF was represented through β, which is related with p_f by Equation 8 (Tan et al., 2013),

$$\beta = \Phi^{-1}(1 - p_f) \quad (8)$$

where Φ^{-1} corresponds to the inverse cumulative standard normal distribution function (Tan et al., 2013). The probability of failure corresponds to the probability that the limit-state function $g(D, S)$ reaches a value less than or equal to zero. The limit-state function was set as the relationship between random variables of strength, S, and demand, D, described in Equation 9 for the SDLS according to the requirements of the NSR-10 (Ministerio de Ambiente Vivienda y Desarrollo Territorial, 2017).

$$g\,(D,S) = S - D = 1\% - \Delta_{máx}\,\% \quad (9)$$

RA considered the uncertainties related to F_s and f_c', the latter relating to E_c (Equation 1) which is associated with the drift. Probability density functions, PDFs, considered for F_s and $f_c'$are presented in Table 2, according to (Beltran and Troncoso, 2010; Bucher and Bourgund, 1990; Montiel and Ruiz, 2007), where μ and $c.o.v.$ correspond to the mean and coefficient of variation of the random variable, respectively. The mean values for the probabilistic variable F_s correspond to the values determined by the EHF method in each iteration.

Considering that $\Delta_{máx}$ is obtained by structural analysis, Equation 9 is an implicit limit-state function. MCS was previously implemented to determine β, using the implicit limit-state function; this implied high computation times, so it was necessary to implement an approximate explicit limit-state function using RSM. β was calculated using the MCS and HL-RF method employing the approximate explicit limit state, getting computationally economical results. For the optimization process incorporating structural reliability, β was constrained to values equal to or greater than 1.75, associated with $p_f = 4.01\%$ following the recommendations of Kim and Wen (1990) and (1987) for the SDLS.

Response Surface Method (RSM)

As previously mentioned, the limit-state function

presented in Equation 9 is implicit; therefore, to reduce computation times in the calculation of β, it was necessary to approximate it through an explicit function. As reported by Tan et al. (2013), Bucher and Bourgund (1990) and Hadidi et al. (2017), this approximate explicit function can be found through the RSM, which considers this function to be a second-order polynomial without cross-terms, as presented in Equation 10 (Hadidi et al., 2017).

$$\hat{g}(y) = a + \sum_{j=1}^{n} b_j \cdot y_j + \sum_{j=1}^{n} c_j \cdot y_j^2 \qquad (10)$$

where y_j are the random variables, n is the number of random variables and a, b_j and c_j are coefficients to be determined. The response surface coefficients were determined using a sample of 2n+1 points, required to adjust the polynomial. Points used were determined using the linear structural analysis and corresponded to a central point, y_{0j}, which matched the mean value of the random variables, μ_j, and 2n points, distanced three times the standard deviation $(\pm 3\sigma_j)$ from the central point, according to Tan et al. (2013).

Monte Carlo Simulation

MCS is a method that allows estimating p_f through the simulation of N random scenarios, where each scenario considers different values for random variables, randomly generated based on their respective PDFs. The p_f is determined as the ratio between the number of scenarios that do not fulfill the limit function, N_f and N, as shown in Equation 11 (Lee and Kim, 2006). This study considered a value of $N = 10^5$, obtained from a convergence analysis of p_f for different values of N.

$$p_f = \frac{N_f}{N} = \frac{N_f}{10^5} \qquad (11)$$

Hasofer-Lind and Rackwitz-Fiessler Method

In order to evaluate a computationally less expensive alternative than the MCS, β was also calculated using the HL-RF method, as recommended in Grubišić et al. (2019), Tan et al. (2013) and Makhduomi (2017). The method uses iterative calculations in a standard normal space; therefore, it requires normalizing the approximate explicit limit-state function and transforming random variables with PDFs different from the normal distribution using the third-moment standardization method. The approximate explicit limit-state function was normalized to obtain the standardized limit-state function shown in Equation 12 (Tan et al., 2013).

$$\hat{g}(Z) = a + \sum_{j=1}^{n} b_j(\mu_j + \sigma_j \cdot Z_j) + \sum_{j=1}^{n} c_j(\mu_j + \sigma_j \cdot Z_j)^2 \qquad (12)$$

where $Z_j$represents the standardized random variable through the expression $Z_j = (y_j - \mu_j)/\sigma_j$, which for normal random variables is equal to the design point U_j defined as the limit surface point in the normalized space closest to the origin (Celorrio Barragué, 2013). As the first step of the iteration process, β and $\mathbb{U}$ were initially assumed as $\beta_0 = 1$ and $\mathbb{U}_0 = (0,0,..,0)$ and then, their values were updated in each iteration, i, according to Equations 13 and 14 (Celorrio Barragué, 2013) until convergence was reached.

$$U_j = \beta_{i-1} \cdot \alpha_j; \quad j = 1, 2, \dots, n \qquad (13)$$

$$\beta_i = \frac{\hat{g}(\mathbb{U}_i) - \sum_{j=1}^{n} \frac{\partial \hat{g}(\mathbb{U}_i)}{\partial U_j} U_j}{\sqrt{\sum_{j=1}^{n} \left[\frac{\partial \hat{g}(\mathbb{U}_i)}{\partial U_j}\right]^2}} \qquad (14)$$

In Equation 13, α_j is the sensitivity coefficient calculated through Equation 15 (Lu et al., 2017).

$$\alpha_j = -\frac{\frac{\partial \hat{g}(\mathbb{U}_{i-1})}{\partial U_j}}{\sqrt{\sum_{j=1}^{n} \left[\frac{\partial \hat{g}(\mathbb{U}_{i-1})}{\partial U_j}\right]^2}} \qquad (15)$$

Third-moment Standardization Method

Considering the intervention of variables with PDFs different from the normal distribution in the calculation of β, the third-moment standardization method proposed by Lu et al. (2017) and Zhao and Ono (2000) was implemented for approximating the standardized random variable by a second-order polynomial, as shown in Equation 16 (Lu et al., 2017).

$$Z_j = f(U_j) = z_{1j} + z_{2j} \cdot U_j + z_{3j} \cdot U_j^2 \qquad (16)$$

In this equation, z_{1j}, z_{2j} and z_{3j} are coefficients of

the second-order approximate polynomial, determined by Equations 17, 18 and 19 (Lu et al., 2017).

$$z_{3j} = sgn(\alpha_{3xj})\sqrt{2}\cos\left[\frac{sgn(\alpha_{3j})\theta_j - \pi}{3}\right] \quad (17)$$

$$z_{1j} = -z_{3j} \quad (18)$$

$$z_{2j} = \sqrt{1 - z_{3j}^2} \quad (19)$$

$$\theta_j = \tan^{-1}\left(-\frac{\sqrt{8 - \alpha_{3j}^2}}{\alpha_{3j}}\right) \quad (20)$$

where α_{3j} is the third statistical moment (coefficient of skewness) of each random variable calculated using Equation 20 (Lu et al., 2017).

Heuristic Optimization Methods

HO methods, according to Kunche and Reddy (2016) and Wang and Chen (2013), provide a computational procedure that determines an optimal solution that maximizes or minimizes an objective function $f(x)$, iteratively improving a candidate solution (x) according to an established quality measure, consisting of optimization variables, at a reasonable computational cost, making no or few assumptions about the problem covered. This study carried out HO using the toolbox of the MATLAB® 2019b software. The methods used were PSO and GA, implemented using the MATLAB® 2019b functions "particlesswarm" and "GA", respectively.

Objective Function

The objective function corresponded to the weight of the RCPF, consisting of plain concrete, $\rho_c = 2300\ kg/m^3$ and longitudinal rebar, $\rho_s = 7800\ kg/m^3$ (Ministerio de Ambiente Vivienda y Desarrollo Territorial 2017). Constraints were incorporated into the objective function using the penalty method, adding a term to the objective function corresponding to the product between the penalty parameter, μ_p, and the penalty function, $p(x)$, in accordance with Masuda et al. (2010). Equation 21 presents the objective function used, where $V_{Concrete}$ and V_{Steel} correspond to the volume of concrete and steel, respectively.

$$f(x) = V_{Concrete} \cdot 2300\ kg/m^3 + V_{Steel} \cdot 7800\ kg/m^3 + \mu_p \cdot p(x) \quad (21)$$

Optimization Variables

Optimization variables, OV, corresponded to the dimensions and longitudinal rebar of the cross-sections, as shown in Table 3. The cross-sections of the structural elements of the RCPF presented in Fig. 1, considered in the minimization of weight, were the initial, midspan and end sections for the beams and a single section for each column. In total, 66 optimization variables were used. In addition, according to commercial availability and construction criteria, allowable dimensions of the cross-sections were rounded to multiples of 5 mm, the diameters to multiples of 3.175 mm and the amount of rebar to integers.

Penalty Method

The penalty method allowed the constrained optimization problem, described by Equation 22 (Masuda et al., 2010), to be developed from an unconstrained optimization approach, as shown in Equation 23 (Masuda et al., 2010), incorporating a penalty parameter and a penalty function. Constrained and unconstrained approaches are equal when all constraints are met and, in turn, null penalties are obtained.

$$\min_{x \in D} f(x);\ Subject\ to\ g_m(x) \leq 0, m = 1, \ldots, M \quad (22)$$

In Equation 22, $g_m$represents the design constraints associated with optimization variables, (x) and M is the number of constraints.

$$P(\mu) = \min_{x \in D} \emptyset\,(x, \mu) = f(x) + \mu_p \cdot p(x) \quad (23)$$

In Equation 23, μ_p and $p(x)$ are the penalty parameter and the penalty function, respectively.

This study considered two alternatives $p(x)$, shown in Equations 24 and 25 (Masuda et al., 2010), which are continuous, equal to zero if $x \in S$ or greater than zero if $x \notin S$, where $S = \{x | g_m(x) \leq 0, m = 1, \ldots, M\}$.

$$p_1(x) = \sum_{m=1}^{M} \max\{0, g_m(x)\} \quad (24)$$

$$p_2(x) = \frac{1}{2}\sum_{m=1}^{M} \max\{0, g_m(x)\}^2 \quad (25)$$

Incorporated constraints considered in sections A, B and C of the NSR-10 are structural requirements for the design of reinforced-concrete structures, including the control of the resistance in the joint according to C.21.6.2.2 to prevent a column-failure mechanism that can lead to collapse and the control of the story drift. Finally, to select the values of μ_p and the $p(x)$ function to be used to obtain the final optimization results, preliminary simulations were performed with Equations 24 and 25 and μ_p values were between 1 and 2000.

Particle Swarm Optimization-PSO

PSO is an optimization algorithm that repeatedly modifies a swarm of particles representing candidate solutions, where the success of a particle is affected not only by its effort, but also by information shared with all swarm particles. In each iteration, the algorithm modifies the velocity of the particles and updates their positions. The position of a particle is denoted x_i and determined by Equation 26 (Kennedy and Eberhart, 1995), where x_{i-1} corresponds to its previous position and v_i to its current velocity.

$$x_i = x_{i-1} + v_i \tag{26}$$

In each iteration, velocity is determined using Equation 27 (Ben Ali, 2012), where w is the inertia weight, v_{i-1} is the previous velocity, $c_1 = 2$ is the weighting of the best position of each particle, P_i is the best position of the particle up to the current iteration, $c_2 = 2$ is the weighting of the best swarm position and P_g is the best swarm position until the current iteration (Ab. Aziz et al., 2011). Rand represented a random number between 0 and 1 and the value of w ranged from 0.4 to 0.9 (Ben Ali, 2012).

$$v_i = w \cdot v_{i-1} + \mathrm{c}_1 \cdot rand \cdot (P_i - x_i) + \mathrm{c}_2 \cdot rand \cdot (P_g - x_i) \tag{27}$$

PSO flowchart implemented in the MATLAB® 2019b software toolbox is shown in Fig. 5.

Genetic Algorithm-GA

GA repeatedly modifies a population of individuals representing candidate solutions. In each generation, the algorithm randomly selects individuals from the current population used as parents to produce new candidate solutions, known as children, that make up the next generation. The succession of generations allows the evolution of the population towards an optimal solution (Mathworks, 2019).

The selection of parents to create the children was made using the selection function 'selectionroulette' implemented by Huang et al. (2021), which simulates a roulette wheel where each individual is assigned a section with an area proportional to its fitness and generates random numbers to select sections and in turn, the individuals attended to be parents (Mathworks, 2019). The next-generation offspring are created according to the reproduction options, as illustrated in Fig. 6 (Mathworks, 2019).

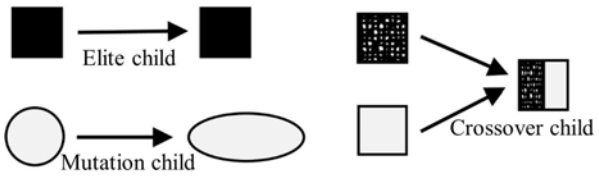

Figure (6): Types of children in the new generation (Mathworks, 2019)

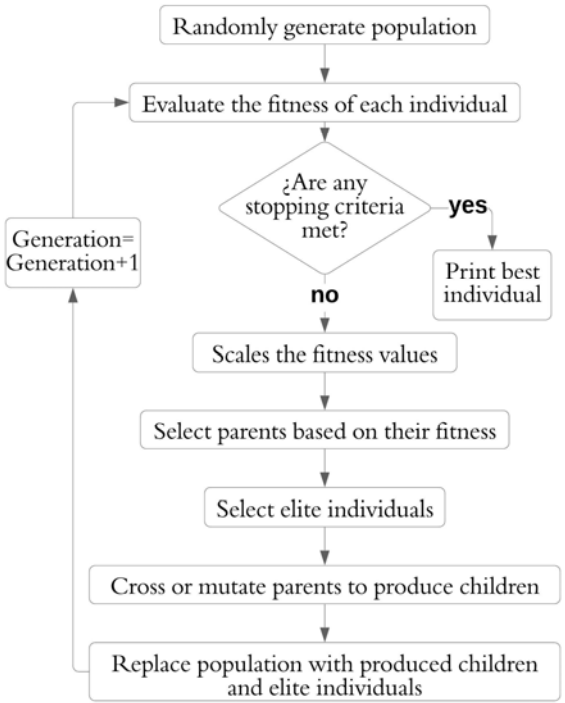

Figure (7): GA flowchart (Mathworks, 2019)

In GA, the number of individuals guaranteed to survive until the next generation is specified by 'EliteCount. 'CrossoverFraction' represents the fraction

of children produced by crossing through the 'crossoversinglepoint' function (Huang et al., 2021), which generates a random number, n, between 1 and the number of optimization variables, to concatenate the first n terms of the first parent with the numbered terms greater than n of the second parent. Finally, the remaining offspring are produced by mutation, applying random changes to a single individual in the current generation to create offspring. The GA flowchart used in this work is shown in Fig. 7 and was implemented in the MATLAB® 2019b software toolbox.

The automatic seismic design procedures (ASDP) flowchart employed in this work are presented in Fig. 8.

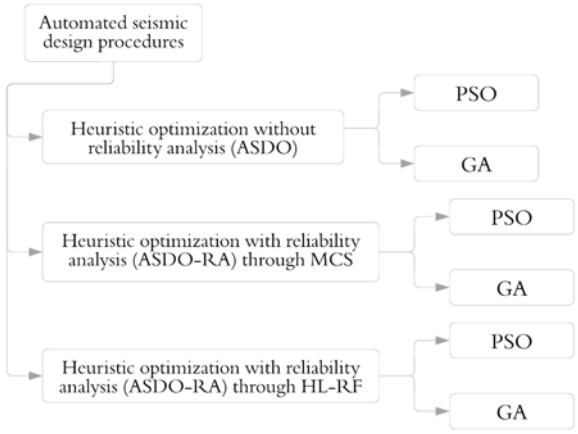

Figure (8): Automatic seismic-design procedures' flowchart (ASDP)

Optimization Scenarios

Two general optimization scenarios (I) and (II), divided in six optimization procedures (i-vi) and one conventional design (vii), described in Table 4, were executed to evaluate the impact of incorporating RA into structural optimization. In ASDO-RA procedures (i)-(iv), the explicit limit-state function was considered through RSM, which in preliminary calculations presented percentage errors between 4.09E-14 and 3.66E-2 for the implicit limit-state function, validating its implementation.

The limits of the search space, which describes the values that candidate solutions can take, used in all optimization scenarios, are shown in Table 5, according to the optimization variables (OV) and their respective units declared in Table 3. These limits were defined according to the minimum depth beam to meet the deflection criteria proposed in C.9.5.2.1 and minimum dimensions for columns, C.21.6.1.1. as per the NSR-10.

In order to contrast results under equivalent parameters, the values used for the swarm or population were 1000 particles or individuals, the stop criteria corresponding to the maximum number of iterations or generations were 1000, according to Masuda et al. (2010) and the minimum relative change in the objective function was 0.001 at a maximum of 50 iterations for all six optimization procedures. Additionally, the 'useparallel' option was employed to perform calculations of the objective function in parallel.

Table 4. Optimization scenarios. β refers to the reliability index, which measures structural reliability. NA: not applicable

Scenario	Procedure		β min constraint	\β calculation method
(I)	(i)	ASDO-RA (PSO)	YES	HL-RF
	(ii)	ASDO-RA (GA)	YES	HL-RF
	(iii)	ASDO-RA (PSO)	YES	MCS
	(iv)	ASDO-RA (GA)	YES	MCS
(II)	(v)	ASDO (PSO)	NOT	NA
	(vi)	ASDO (GA)	NOT	NA
Office work	(vii)	Conventional	NO	NA

Table 5. Search space

OV		1	2	3	4	5	6	7
Limits	Lower	300	0.72	5	400	600	5	4
	Upper	550	0.85	6	700	800	8	30

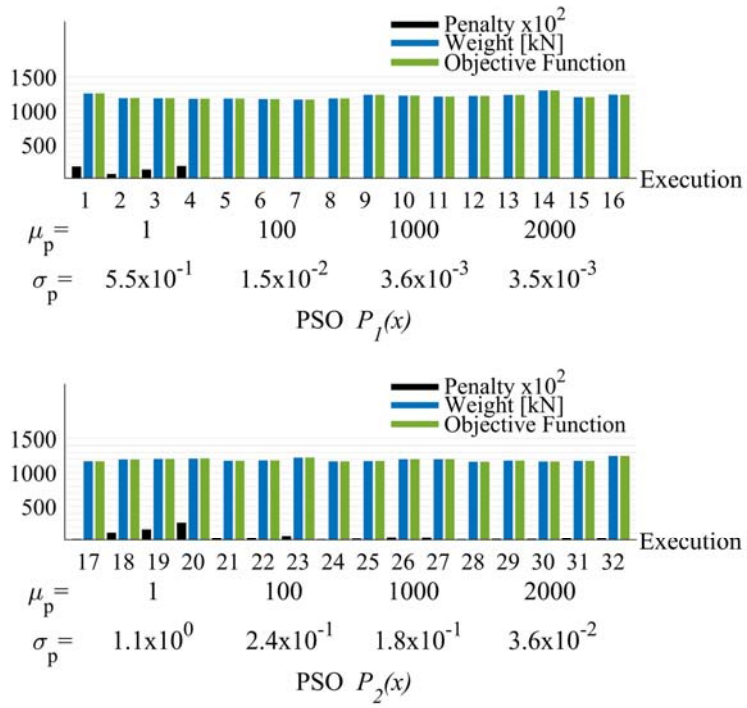

a) PSO

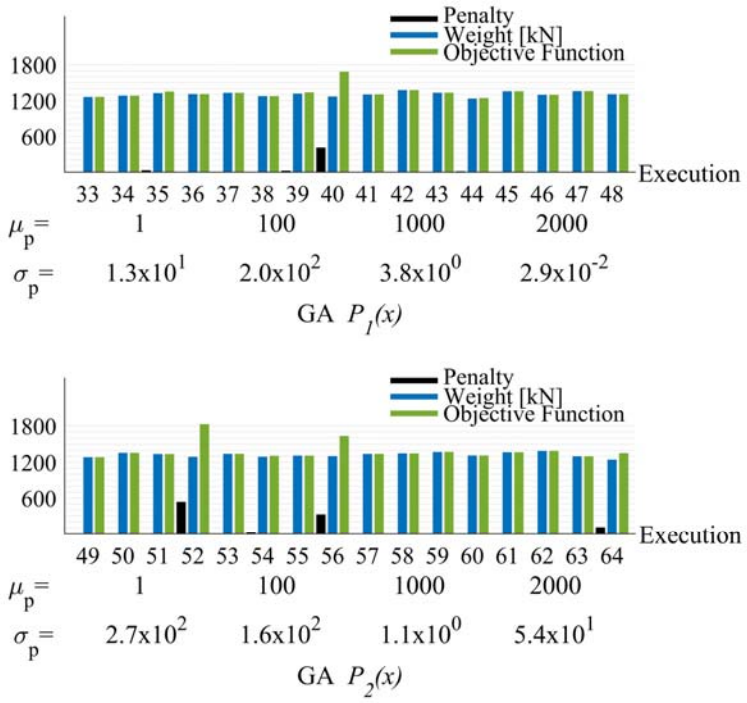

b) GA

Figure (9): Preliminary executions of optimization procedures. a) PSO and b) GA

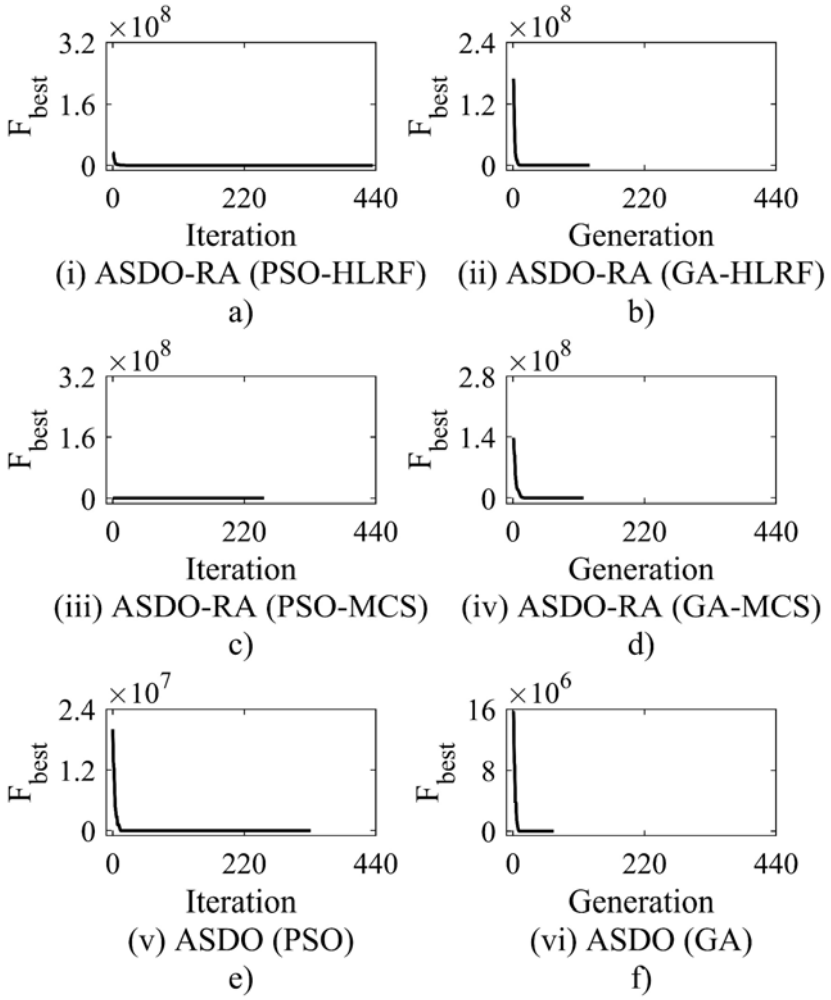

Figure (10): Convergence curves of the best execution for each optimization scenario according to ASDP

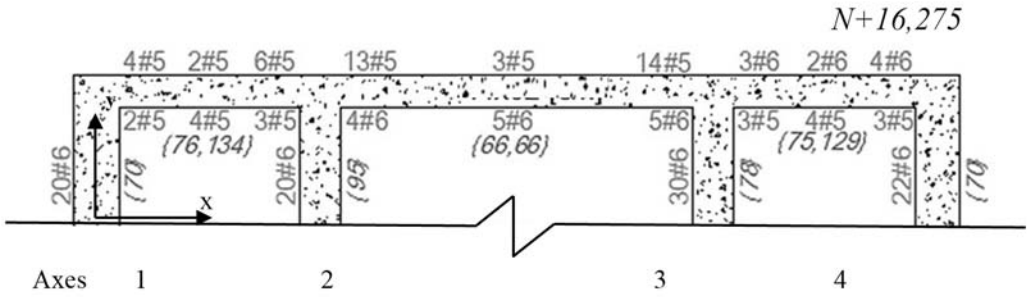

Figure (11): Reinforcement details of the optimum design obtained using ASDO-RA HL-RF for the level N+16.175 of the RCPF studied

The following performance measures were used to evaluate and compare the results of the different optimization scenarios: penalty, P, which in order to express only the value of constraints that are not satisfied, corresponds to $P = \mu_p \cdot p(x) = 1;\cdot p_1(x)$ and standard deviation in the penalty, σ_p measures the degree of dispersion or variability.

All the above-described procedures were carried out using the authors-made codes in the MATLAB® 2019b software and the implementation of the toolbox for optimization available in it. Optimizations were performed on two personal laptops with Core i5-8250U,

1.6 GHz, 8 GB RAM and AMD Ryzen 5 3500U, 2.1 GHz, 12 GB RAM.

ASDP NUMERICAL RESULTS AND DISCUSSION

Conventional Structural Design

Based on the code developed by the authors in the MATLAB® 2019b software and to estimate the percentage variations of the results of each optimization scenario, a conventional structural design of the RCPF was performed. This design was developed as is usual in the design industry in Colombia, using a manual process of trial and error until meeting the applied design code. The time employed in the conventional design was approximately two hours (2 h), for which a weight of 1151.8 kN was obtained, and its cross-sections are subsequently presented in the following sub-sections.

Selection of Penalty Parameter and Penalty Function

The penalty parameter and penalty function implemented in the objective function were established according to preliminary executions of optimization procedures (i) and (ii) according to Table 4. The penalty functions $p_1(x)$ and $p_2(x)$ were evaluated with $\mu_p = [1{,}100{,}1000{,}2000]$, performing four executions in each test case. Fig. 9 shows the penalty, weight and objective function values for the executions for each test case, along with the corresponding μ_p and $\boldsymbol{\sigma_p}$.

The best weight values, associated with null penalties, correspond to executions no. 6 and no. 46, having weights of 1173.9 kN and 1300.1 kN, respectively. However, these are obtained by different penalty parameters. Considering the above and the need to select an equal penalty function and penalty parameter for both algorithms (GA and PSO), these are set to $p_1(x)$ as recommended by Masuda et al. (2010), Wang et al. (2021) and Xia et al. (2019) and $\mu_p = 2000$ which generate penalty results very close to zero, with σ_p 3.5E-3 and 2.9E-2, in PSO and GA together.

Optimized Structural Designs

Due to the stochastic nature of the algorithms used, ten executions of each optimization procedure were performed, as recommended by Masuda et al. (2010). The convergence curves are shown in Fig. 10, where F_{best} corresponds to the best value of the objective function.

From there, it is possible to infer that the PSO and GA algorithms, as exposed by Ab. Aziz et al. (2011) and Dillen et al. (2021) previous investigations, successfully solve the proposed optimization problem in several iterations/generations below the established limit, the stop criterion of the executions being the minimum relative change of the objective function in all cases. The optimization times were between 0.180 hour and 9.079 hours, which are relatively low and attractive to their structural design implementation.

Table 6 presents the penalty value, weight, execution time and number of iterations/generations corresponding to the best result of each procedure according to the ASDP performed using $p(x)$ and μ. The convergence curves of these executions corresponding to the best results are presented in Fig. 10. All six optimization procedures had null penalties, which means that all the design criteria were met and in turn, the optimization problems in Equations 20 and 21 were equivalent. This evidences that the penalty-method approach is feasible for solving constrained optimization problems. Additionally, the six optimization procedures have significantly low values of σ_p (between 7.7E-4 and 9.9E-2), except for scenario (iv) with $\sigma_p = 62$.

The better performance of the PSO algorithm in weight minimization, in contrast to the GA algorithm, evidenced in the executions mentioned above, can be explained by the larger number of iterations and longer computational times presented in the PSO algorithm. Therefore, it is recommended to modify the stop criteria of the GA algorithm in order to increase the number of generations evaluated and improve its performance. The best result for each calculation method of β was selected following the performance measures (Table 4; these will be referred to from now on as scenarios (or results) I (HL-RF), II (MCS) and III (not applicable, NA), according to the calculation method used and corresponded to the executions number 7, 26 and 42 of the PSO algorithm, presented in Table 6, which had 435, 253 and 331 iterations and 2.19E-2, 6.76E-2 and 1.05E-2 seconds per design, respectively. In addition, the result of the conventional structural design (scenario IV) will be referred to as result IV (conventional). The results I (HL-RF), II (MCS) and III (NA) have RCPF with weights of 1205.8 kN, 1262.6 kN and 1080.2 kN and percentage variations from result IV (conventional) of

+4.69%, +9.62% and -6.22%, respectively. The latter mentioned percentage is reported by other researchers (Tsiptsis et al., 2019). According to the percentage increase in results, I (HL-RF) and II (MCS) for result IV (conventional), it is recommended to consider structural RA even if optimization is not intended in order to meet the β proposed limit.

The description of the longitudinal and transverse rebar of beams and columns of the optimum design obtained using ASDO-RA HL-RF for the level N+16.175 m of the RCPF studied is shown in Figure 11. Rebar diameters in beams (positive and negative) and columns in Figure 11 were indicated by ***d#c*** (i.e., ***d*** bars number ***c***) and the separation of stirrups (in mm) in beams and columns were denoted between parentheses (confined and not confined areas). Table 7 presents the RCPF designs using ASDP corresponding to results I-IV; these outcomes include the dimensions of the cross-sections and the description of the longitudinal and transverse rebar. Additionally, as presented in Table 7, the value of the weight, $\beta_{critical}$ and $\beta_{theoretical\ critical}$, along with their respective associated probability of failure p_f are shown. $\beta_{critical}$ is the lowest value of β obtained in each RCPF design, which corresponded to N+6.975 story and $\beta_{theoretical\ critical}$ is the lowest value of β obtained in each RCPF through the MCS method implementing the implicit and accurate limit-state function (Tan et al., 2013).

Table 6. The best results of scenarios (I) and (II) ASDP executions according to the β calculation method employed

Scenario	σ_p	N°.	P	Weight [kN]	Time [h]	Iteration	Scenario	σ_p	N°.	P	Weight [kN]	Time [h]	Generation
(i) HL-RF	3.0E-2	7	0.0000	1205.8	2.643	435	(ii) HL-RF	9.1E-2	17	0.0000	1300.1	0.670	128
(iii) MCS	3.9E-2	26	0.0000	1262.6	4.748	253	(iv) MCS	6.2E+1	32	0.0000	1364.4	2.000	118
(v) NA	7.7E-4	42	0.0000	1080.2	0.969	331	(vi) NA	9.9E-2	51	0.0000	1160.6	0.300	68

Table 7. RCPF structural designs using ASDP

ASDP Scenarios	RCPF Weight (kN)	β theoretical critical and *pf*	βcritical and *pf*	Floor levels [m]	Beam width [mm]	Beam depth [mm]	Column axes	Column width [mm]	Column depth [mm]	Column rebar diameter [in/8]
I. ASDO-RA HL-RF	1205.8	1.534 6.25%	1.753 3.98%	N+16.275	440	520	1	475	800	6
				N+13.275	405	560	2	665	720	6
				N+10.125	435	600	3	665	720	6
				N+6.975	550	765	4	475	800	6
				N+2.525	540	750	-	-	-	-
II. ASDO-RA MCS	1262.6	1.713 4.34%	1.758 3.94%	N+16.275	395	550	1	565	690	5
				N+13.275	405	565	2	700	800	7
				N+10.125	425	590	3	700	800	7
				N+6.975	550	765	4	565	690	5
				N+2.525	525	730	-	-	-	-
III. ASDO	1080.2	0.065 47.41%	-	N+16.275	405	530	1	565	600	5
				N+13.275	440	540	2	565	700	5
				N+10.125	415	575	3	565	700	5
				N+6.975	545	755	4	565	600	5
				N+2.525	510	705	-	-	-	-
IV. Conventional	1151.8	0.068 47.29%	-	N+16.275	410	570	1	590	660	5
				N+13.275	430	590	2	590	750	6
				N+10.125	490	640	3	590	750	6
				N+6.975	540	690	4	590	660	5
				N+2.525	500	620	-	-	-	-

As shown Table 7, the value of $\beta_{theoretical\ critic}$ results for scenarios I (ASDO-RA HL-RF) and II (ASDO-RA MCS) are less than the limit proposed by Kim and Wen (1990) and (1987); however, for result

executions, the alternative method of calculating β resulted in values of $\beta_{critical}$ greater than the limit, these being equal to 1,753 and 1,758, respectively, which can be caused by the accuracy of β alternative calculation methods and the approximate explicit limit-state function using the RSM as evidenced by Makhdoumi et al. (2017). Based on this, it is recommended to increase the value of the proposed limit when implementing β alternative calculation methods, HL-RF and MCS. MCS method corresponding to result II (ASDO-RA MCS) is more accurate than the HL-RF method corresponding to result I (ASDO-RA HL-RF), in computational times 97.2% higher, presenting maximum percentage errors in the value of β, compared to the theoretical β, corresponding to +2.92% and +14.38%, respectively.

Alternative methods HL-RF and MCS used in procedures (i) and (iii) are computationally efficient, according to the maximum percentage errors of β and the average reduction in computational times in contrast to the theoretical method, corresponding to 99.90% and 99.80%, respectively. The incidence of structural reliability, for the SDLS, on optimizations of results I and II contrasted with result III, which does not incorporate structural RA, as can be evidenced by the increase in the cross-section areas of the structural elements and in the percentage increases in weight corresponding to 11.63% and 16.89%, respectively, where the difference between them may arise from the accuracy of β calculation methods mentioned above.

Results III (ASDO) and IV (conventional), which do not incorporate structural RA, have values of $\beta_{theoretical\ critical}$ of 0.065 and 0.068 and considerably high p_f (47.41% and 47.29%, respectively), reiterating that results I-IV meet all the criteria of the applied design code; so not considering reliability in the SDLS can lead to high failure probabilities, which implies damage to non-structural elements to near-collapse of the structure according to FEMA (2012) and Pan American Health Organization (2000). Since only the SDLS was assessed, structural RA importance may be further evident when assessing other limit states.

CONCLUSIONS

As stated in this work, using ASDO-RA for the SDLS in structural design optimization significantly increases the cross-sectional areas of the RCPF studied with respect to the structural design optimization that does not incorporate RA (ASDO). The resulting increases in weight were 11.63% (for the ASDO-RA HL-RF) and 16.89% (for the ASDO-RA MCS) compared to the ASDO.

Even if optimization is not sought (conventional design), it is recommended to guarantee safety by incorporating reliability analysis, because the conventional design and the ASDO, developed here only for the minimum requirements proposed by the NSR-10, presented values of reliability index lower than the limit proposed by Kim and Wen (1990) and (1987).

To promote the incorporation of reliability analysis in structural optimization, the present study proposed a computationally efficient methodology to calculate reliability indices, using the response surface method to approximate the limit-state function, in conjunction with HL-RF or MCS. This methodology proved to be a good alternative, since it resulted in lower execution times (decrease by 99.8%) and low errors (14.4% and 2.9%) when compared to the classic methodology that uses MCS method on the implicit and exact limit-state function.

Finally, regarding to the optimization process, the ASDO-RA (using PSO) achieved the best performance, with optimal weights between 1205.8 kN and 1262.6 kN and the corresponding execution times were between 0.97 h and 4.75 h, which makes it attractive for implementation in the design of actual RCPFs when compared with the two hours used in conventional structural design. Nonetheless, it was found that for any particular structural design problem, the penalty parameter must be adequately determined through preliminary numerical tests before executing optimization.

RECOMMENDATIONS

For future studies, it is recommended to:

- Evaluate the performance of other methods of HO or hybrid versions; i.e., simulated annealing, optimization by ant colony (ACO) and taboo search (TS), to assess their performance in real-life structural design scenarios.
- Use different calculation methods of reliability index, such as gradient projection, augmented Lagrangian, sequential quadratic programming and

the modified HL-RF, among others, to increase the accuracy of the results and reduce computational times.

- Incorporate non-linearity into the limit-state surface and statistical uncertainties associated with other variables (i.e., dead load, cross-sectional area, second moment of inertia and density of materials).
- Consider the impact of structural RA on different limit states, include the foundation's design and weight in the objective function and analyze 3D buildings.

ACKNOWLEDGMENTS

The authors of this work are grateful for the financial support from the Universidad Industrial de Santander-UIS and the INME-UIS research group.

REFERENCES

Ab. Aziz, N.A., Mohemmed, A.W., Alias, M.Y., and Ab Aziz, K. (2011). "Particle- swarm optimization for constrained and multi-objective problems: A brief review". 2011 International Conference on Management and Artificial Intelligence, 6, 146-150. http://www.ipedr.com/vol6/29-A10025.pdf

Aguirre-Guerrero, A.M., and Mejía de Gutiérrez, R. (2020). "Alkali-activated protective coatings for reinforced concrete exposed to chlorides". Construction and Building Materials, 268, 1-15.

Beltran, O., and Troncoso, F. (2010). "Análisis de confiabilidad de la metodología NSR-98 para columnas y vigas estructurales". Tesis de pregrado, Universidad de Sucre. http://repositorio.unisucre.edu.co/handle/001/659

Ben Ali, Y.M. (2012). "Psychological model of particle-swarm optimization-based multiple emotions'. Applied Intelligence, 36 (3), 649-663.

Bucher, C.G., and Bourgund, U. (1990). "A fast and efficient response surface approach for structural reliability problems". Structural Safety, 7 (1), 57-66.

Celorrio Barragué, L. (2013). "Metodología eficiente de optimización de diseño basada en fiabilidad aplicada a estructuras". Tesis doctoral, Universidad de La Rioja.

Danesh, M. (2019). "Evaluation of seismic performance of pbd-optimized steel moment frames by means of neural network". Jordan Journal of Civil Engineering, 13 (3), 472-488.

Dillen, W., Lombaert, G., Mertens, R., Van Beurden, H., Jaspaert, D., and Schevenels, M. (2021). "Optimization in a realistic structural engineering context: Redesign of the market hall in Ghent". Engineering Structures, 228, 1-18.

Faes, M.G.R., and Valdebenito, M.A. (2020). "Fully decoupled reliability-based design optimization of structural systems subject to uncertain loads". Computer Methods in Applied Mechanics and Engineering, 371, 1-17.

FEMA. (2012). "Seismic-performance assessment of buildings (Vol. 1-Method)".

Grubišić, M., Ivošević, J., and Grubišić, A. (2019). "Reliability analysis of reinforced-concrete frame by finite-element method with implicit limit-state functions". Buildings, 9 (5), 1-22.

Hadidi, A., Azar, B.F., and Rafiee, A. (2017). "Efficient response-surface method for high-dimensional structural reliability analysis". Structural Safety, 68, 15-27.

Huang, W., Song, B., Liang, J., Niu, Q., Zeng, G., Shen, M., Deng, J., Luo, Y., Wen, X., and Zhang, Y. (2021). "Design optimization of office-building envelope based on quantum genetic algorithm for energy conservation". Journal of Building Engineering, 35, 1-15.

Kennedy, J., and Eberhart, R. (1995). "Particle-swarm optimization". Neural Networks Proceedings, IEEE International Conference, 4, 1942-1948.

Kim, S.H., and Wen, Y.K. (1987). "Reliability-based structural optimization under stochastic time-varying loads". Doctoral Thesis, University of Illinois.

Kim, S.H., and Wen, Y.K. (1990). "Optimization of structures under stochastic loads". Structural Safety, 7 (2-4), 177-190.

Kunche, P., and Reddy, K.V.V.S. (2016). "Heuristic and meta-heuristic optimization". Metaheuristic Applications to Speech Enhancement, 17-24.

Lee, O.S., and Kim, D.H. (2006). "The reliability estimation of pipeline using FORM, SORM and Monte Carlo simulation with FAD". Journal of Mechanical Science and Technology, 20 (1), 2124-2135.

Li, L., and Liu, F. (2009). “Harmony particle-swarm algorithm for structural-design optimization”. Harmony Search Algorithms for Structural Design Optimization, 121-157.

Li, L., and Liu, F. (2011). “Optimum design of structures with heuristic particle-swarm optimization algorithm”. Group Search Optimization for Applications in Structural Design, 21-67. Springer Verlag, Berlin-Heidelberg.

Lu, Z.-H., Cai, C.-H., and Zhao, Y.-G. (2017). “Structural reliability analysis including correlated random variables based on third-moment transformation”. Journal of Structural Engineering, 143 (8), 1-10.

Luongo, A., D’Annibale, F., and Ferretti, M. (2021). “Shear and flexural factors for static analysis of homogenized-beam models of planar frames”. Engineering Structures, 228, 1-13.

Makhduomi, H., Keshtegar, B., and Shahraki, M. (2017). “A comparative study of first-order reliability method-based steepest descent search directions for reliability analysis of steel structures”. Advances in Civil Engineering, 2017(1), 1-10.

Martinez Molina, W., Torres Acosta, A.A., Alonso-Guzmán, E.M., Chávez-García, H.L., Hernández-Barrios, H., Lara-Gómez, C., Martínez-Alonso, W., Pérez-Quiroz, J.T., Bedolla-Arroyo, J.A., and González-Valdéz, F.M. (2015). “Recycled concrete: A review”. Revista ALCONPAT, 5 (3), 234-247.

Masuda, K., Kurihara, K., and Aiyoshi, E. (2010). “A penalty approach to handle inequality constraints in particle-swarm optimization”. IEEE International Conference on Systems, Man and Cybernetics, 10, 2520-2525.

Mathworks. (2019). "MATLAB® (V. 2019b)". Mathworks. https://www.mathworks.com/

Ministerio de Ambiente Vivienda y Desarrollo Territorial. Comisión Asesora Permanente para el Régimen de Construcciones Sismo Resistentes. (2017). "Reglamento Colombiano De Construcción Sismo Resistente NSR-10". Asociación Colombiana de Ingeniería Sismica. https://asosismica.org.co/producto/reglamento-colombiano -de-construccion-sismo-resistente- nsr-10/

Montiel, M.A., and Ruiz, S.E. (2007). “Influence of structural capacity uncertainty on seismic reliability of buildings under narrow-band motions”. Earthquake Engineering and Structural Dynamics, 36 (13), 1915-1934.

Negrin, I.A., Negrin, A., and Chagoyén, E.L. (2019). “Optimization of reinforced concrete plane frames using a hybridization of genetic algorithms and the Nelder-Mead algorithm”. Obras y Proyectos, 26, 74-86.

Pan American Health Organization. (2000). “Principles of disaster mitigation in health facilities”. PAHO Library. www.paho.org/spanish/ped/pedsres.htm

Peng, Y., Ma, Y., Huang, T., and De Domenico, D. (2021). “Reliability-based design optimization of adaptive sliding base-isolation system for improving seismic-performance of structures”. Reliability Engineering and System Safety, 205, 1-16.

Rajeev, S., and Krishnamoorthy, C.S. (1992). “Discrete optimization of structures using genetic algorithms”. Journal of Structural Engineering, 118(5), 1233-1250.

Rastegaran, M., Aval, S.B.B., and Sangalaki, E. (2022). “Multi-objective reliability-based seismic-performance design optimization of SMRFs considering various sources of uncertainty”. Engineering Structures, 261(March), 114219.

Tan, X. hui, Shen, M. fen, Hou, X. liang, Li, D., and Hu, N. (2013). “Response-surface method of reliability analysis and its application in slope-stability analysis”. Geotechnical and Geological Engineering, 31 (4), 1011-1025.

Tsiptsis, I.N., Liimatainen, L., Kotnik, T., and Niiranen, J. (2019). “Structural optimization employing isogeometric tools in particle-swarm optimizer”. Journal of Building Engineering, 24, 1-12.

Wang, F.-S., and Chen, L.-H. (2013). “Heuristic optimization”. In: Encyclopedia of Systems Biology, 885.

Wang, F., Zhang, H., and Zhou, A. (2021). “A particle-swarm optimization algorithm for mixed-variable optimization problems”. Swarm and Evolutionary Computation, 60, 1-12.

Xia, Y., Feng, Z. kai, Niu, W. jing, Qin, H., Jiang, Z. qiang, and Zhou, J. zhong. (2019). “Simplex quantum-behaved particle-swarm optimization algorithm with application to ecological operation of cascade hydropower reservoirs”. Applied Soft Computing Journal, 84, 1-16.

Zhao, Y.-G., and Ono, T. (2000). “Third-moment standardization for structural reliability analysis”. Journal of Structural Engineering, 126 (6), 724-732.